→ 3rd ADVANCED COURSE ON RADAR POLARIMETRY

Pol SAR App - Urban

Application of polarimetry to urban areas

Elise Koeniguer

Contact:
elise.koeniguer@onera.fr
ONERA
Chemin de la Hunière et des Joncherettes
BP 80100
FR-91123
PALAISEAU CEDEX

Outline

- Introduction: Urban applications
- Polarimetry: specificity of the urban context

- Applications
  - Classification
  - 3D
  - subsidence

Application of polarimetry to urban areas

INTRODUCTION

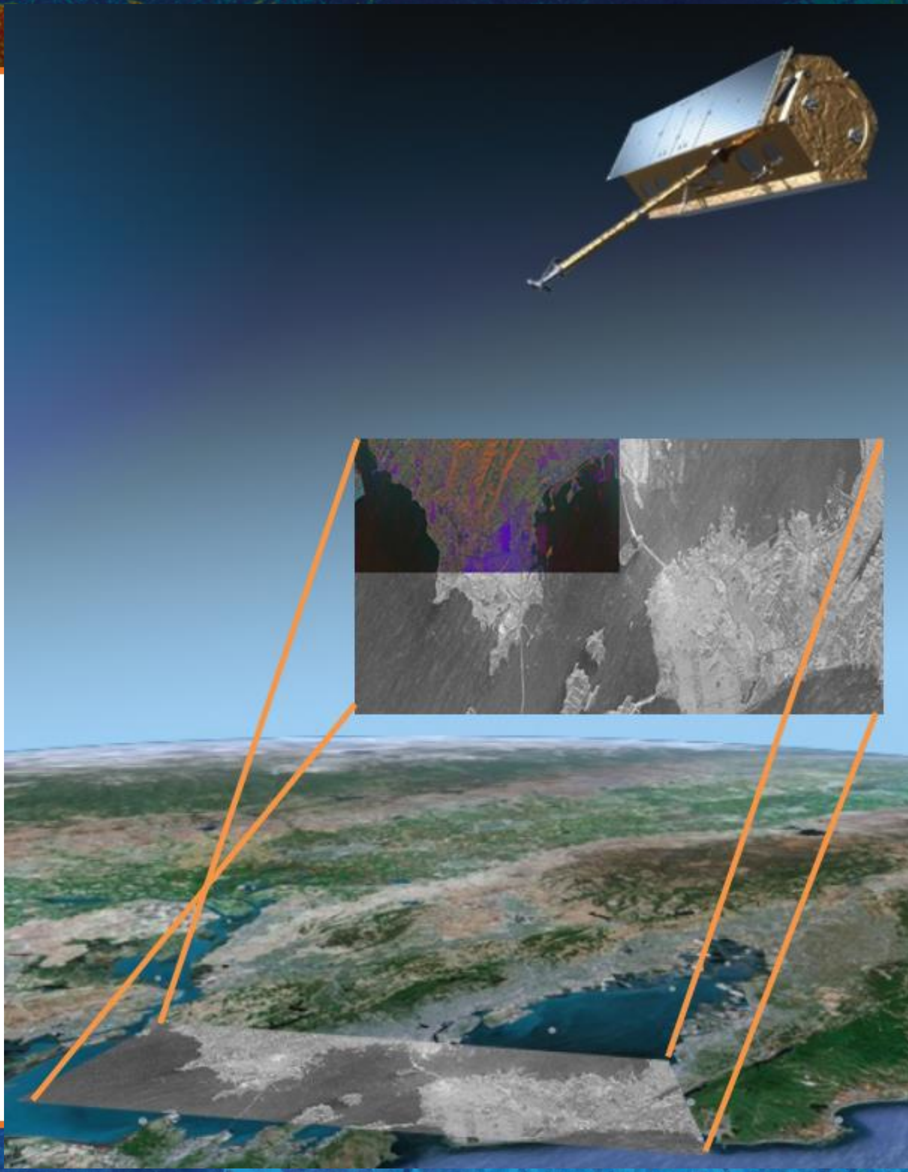

Urban applications

- The world's population is rapidly increasing, especially in urban regions to which many rural inhabitants are migrating
- Results in the need for a efficient method of monitoring cities both in developing and developed countries
- Present monitoring techniques are inefficient and unable to maintain up-to date information
- Demand for settlement detection, urban classification and population estimation.

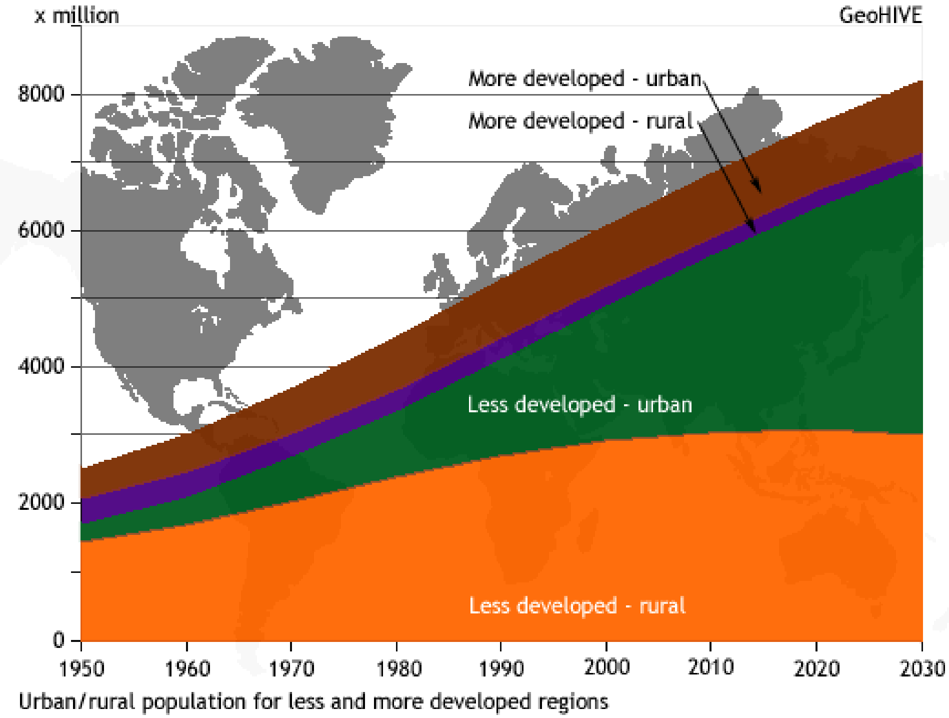

source: Population Division, UN: World Population Prospects

Motivation (1/2)

- Urban environments represent one of the most dynamic regions on earth. Due to these rapid changes, up-to-date spatial information is requisite for the effective management and mitigation of the effects of built-up dynamics.

- Alternative methods as air photo interpretation, national census and related statistics: time consuming, and expensive methods.

- Recent improvement in ground resolution in satellite remote sensing

- Radar benefits: irrespective of the light and weather conditions of the area being imaged.

Showcases on Urban in POLSAR App

APPLICATIONS

Product	Authors (Institution)
Detection of built-up areas	Elise Koeniguer, Nicolas Trouvé (Onera)
Urban classification	Y. Yamaguchi (Niigata University)
3D rendering by POLINSAR	Elise Koeniguer, Nicolas Trouvé (Onera)
3D by tomography	Yue Huang, Laurent Ferro-Famil (IETR Rennes)
Subsidence: ground deformation estimation	Victor D. Navarro-Sanchez, Juan M. Lopez-Sanchez (University of Alicante)
Differential SAR interferometry	Dani Monells, Rubén Iglesias, Xavier Fàbregas, Jordi Mallorquí, Albert Aguasca, Carlos López-Martínez (University of Catalunya)

Application of polarimetry to urban areas

POLARIMETRY IN URBAN

Main mechanisms

Lack of azimuthal symmetry

Orientation angle

Understanding the HV polarization over urban

main classical decompositions

The main mechanisms

- Mixture of single mechanisms
  - First case: h/tan θ > L

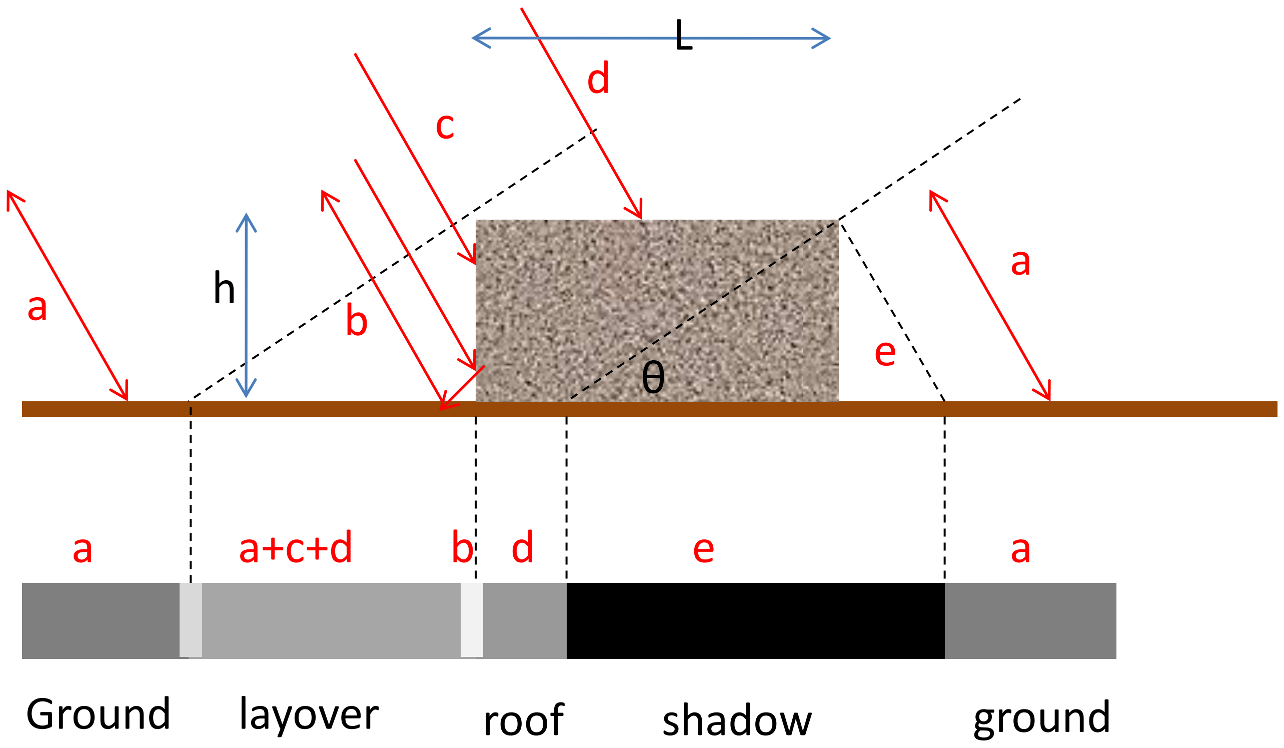

The main mechanisms

- Mixture of single mechanisms
  - First case: $h/\tan\theta < L$

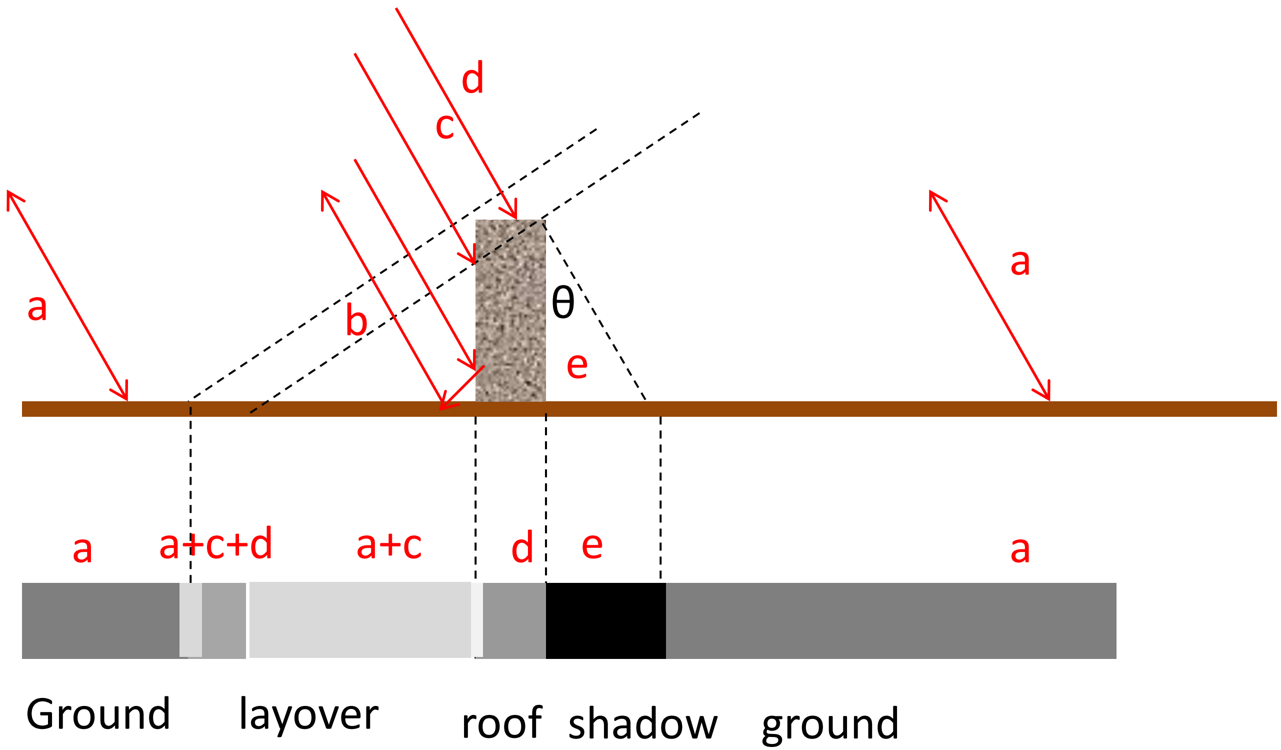

The lack of azimuthal symmetry

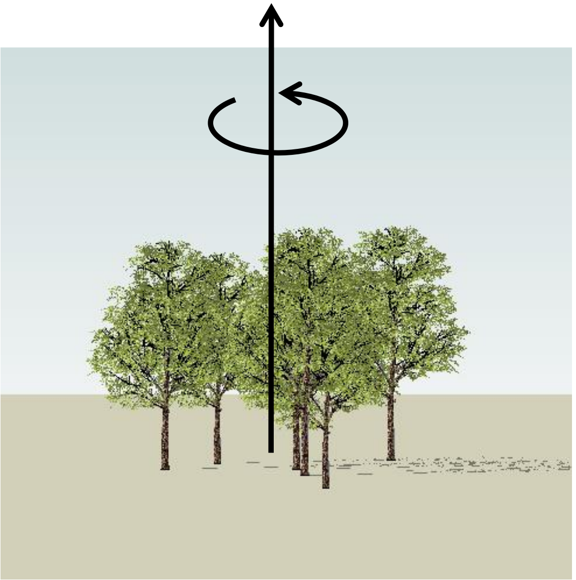

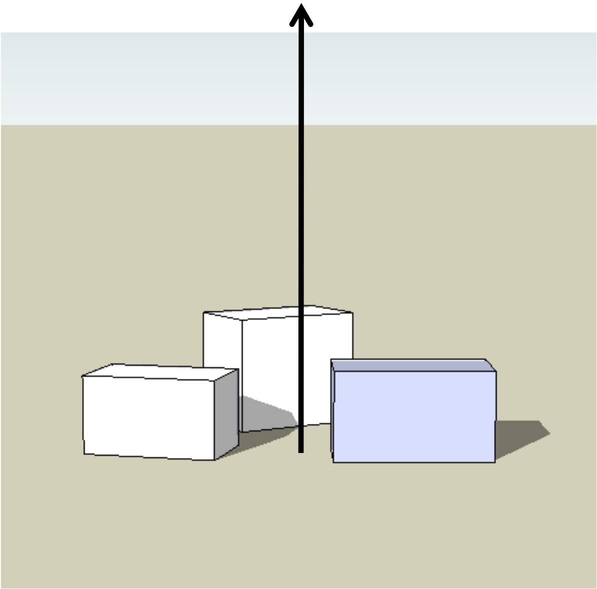

$$< S_{HH}S_{HV}^{*} > = < S_{HV}S_{VV}^{*} > = 0$$

$$< S_{HH}S_{HV}^{*} > \neq 0, < S_{HV}S_{VV}^{*} > \neq 0$$

Example over Pi-SAR data

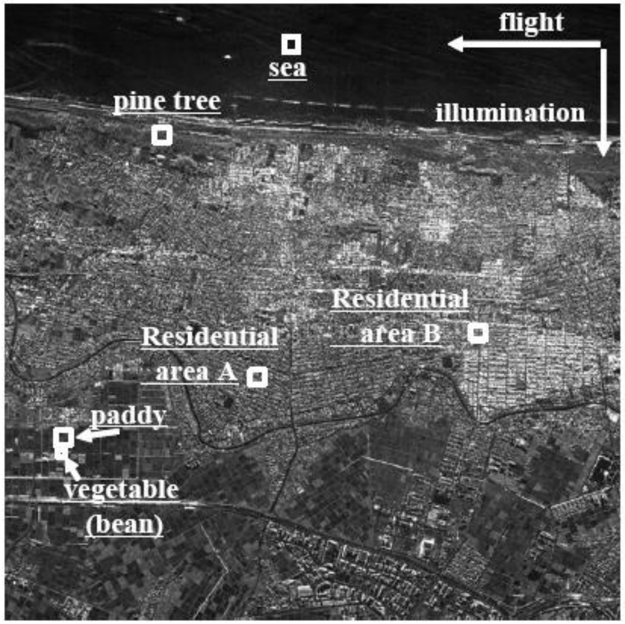

(a) Cor(HH,HV)

(b) Cor(HV,VV)

(c) Cor(RR,LL)

The orientation angle

Induced either by:
- tilted roof
- dihedral effects non aligned with the azimuth

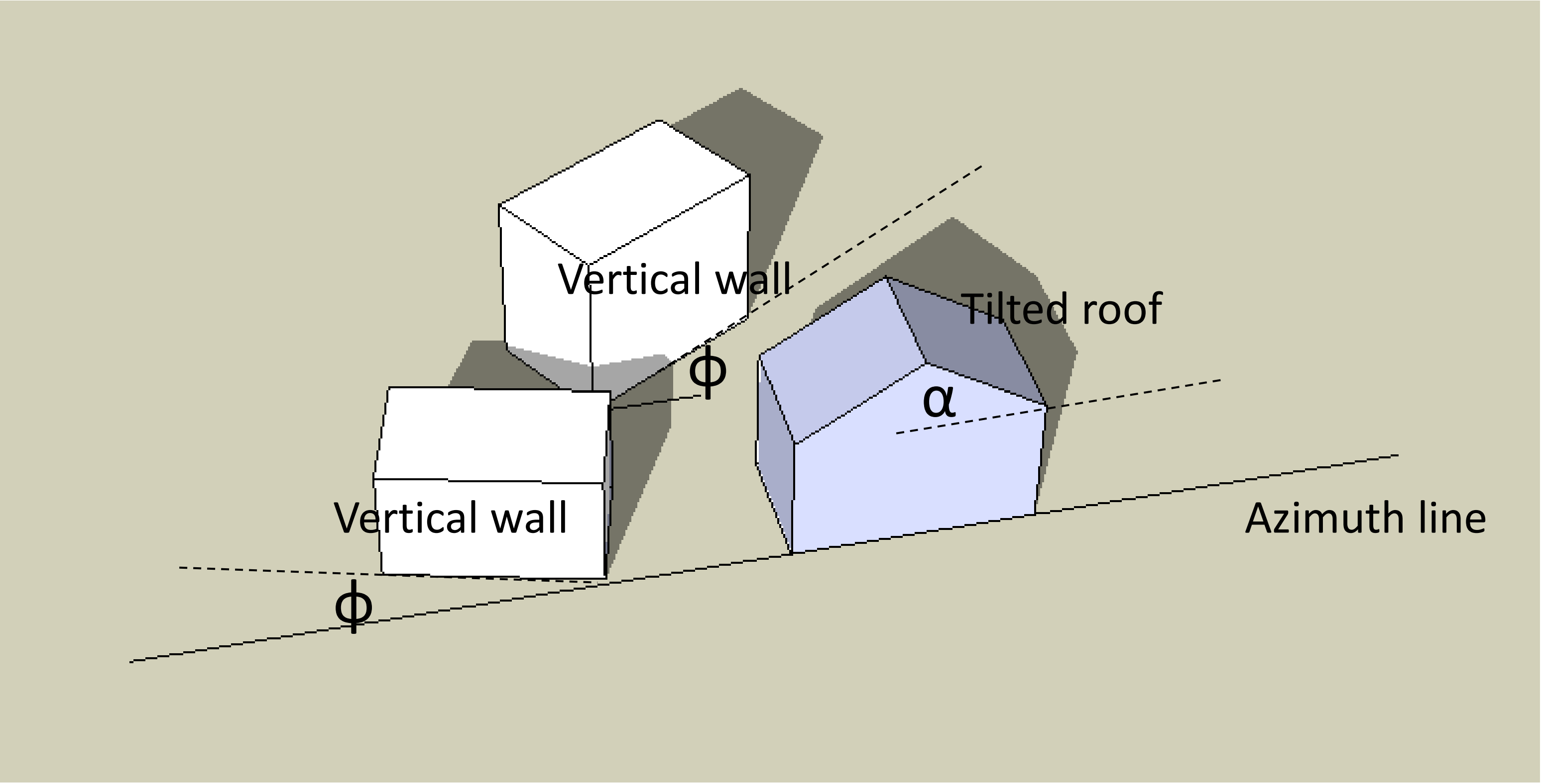

Orientation angle of PiSAR L-band

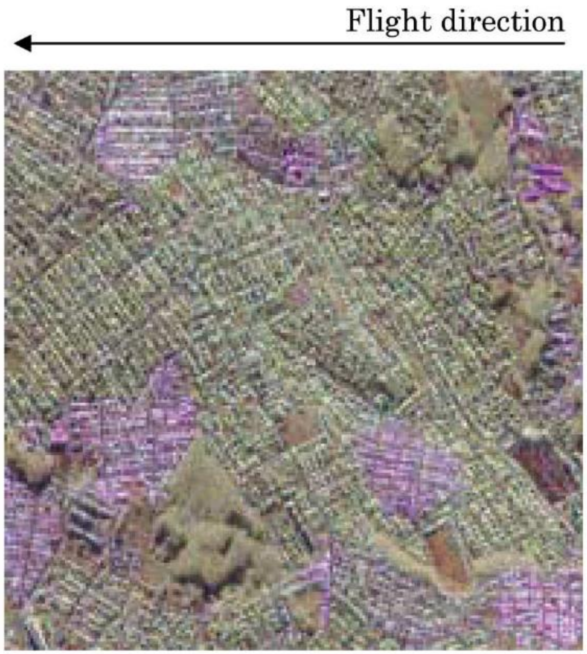

(a)

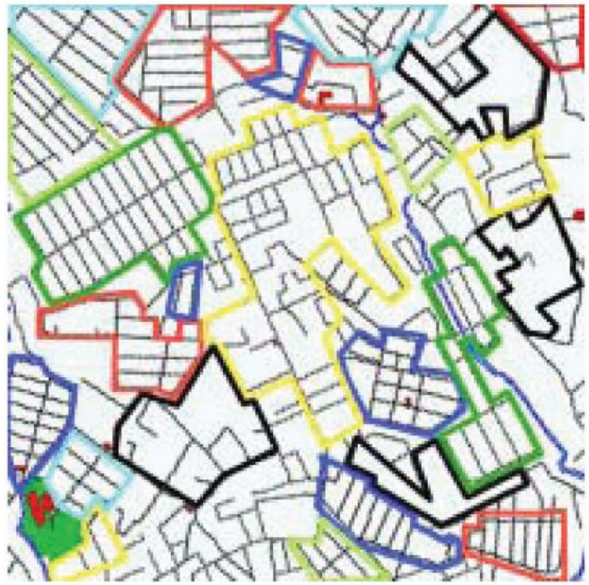

(b)

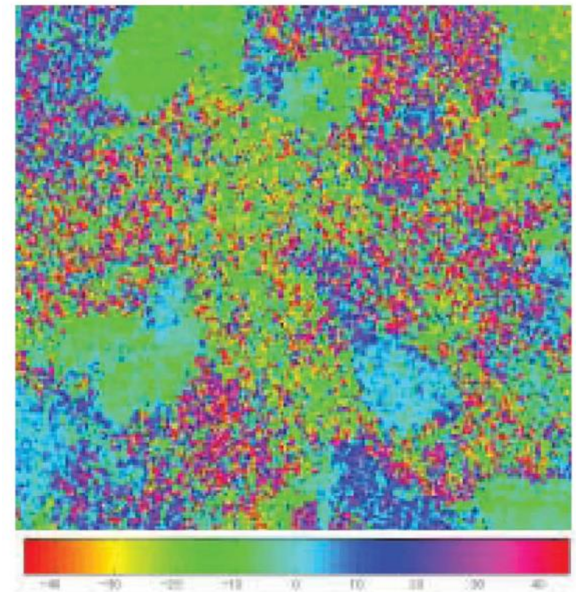

(c)

Fully polarimetric image of a built-up housing area

(Sendaï)

Street pattern. Areas surrounded by the same colored lines possess similar alignment

Polarization orientation angle shifts computed from the polarimetric SAR data

Examples of POA over San Francisco images

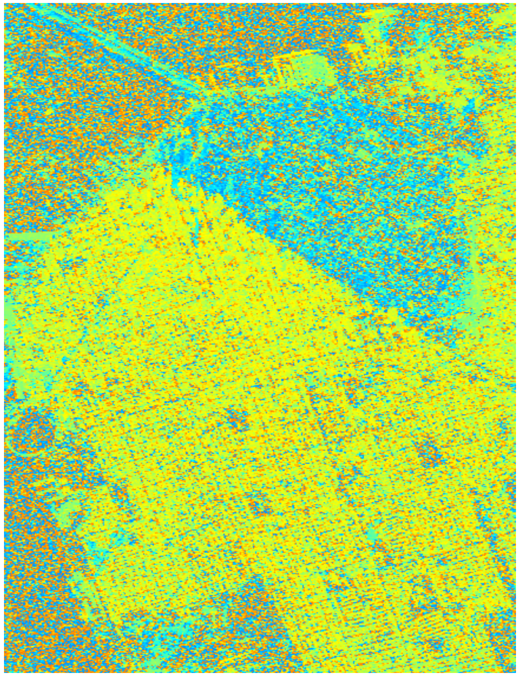

X-band TerraSAR-X

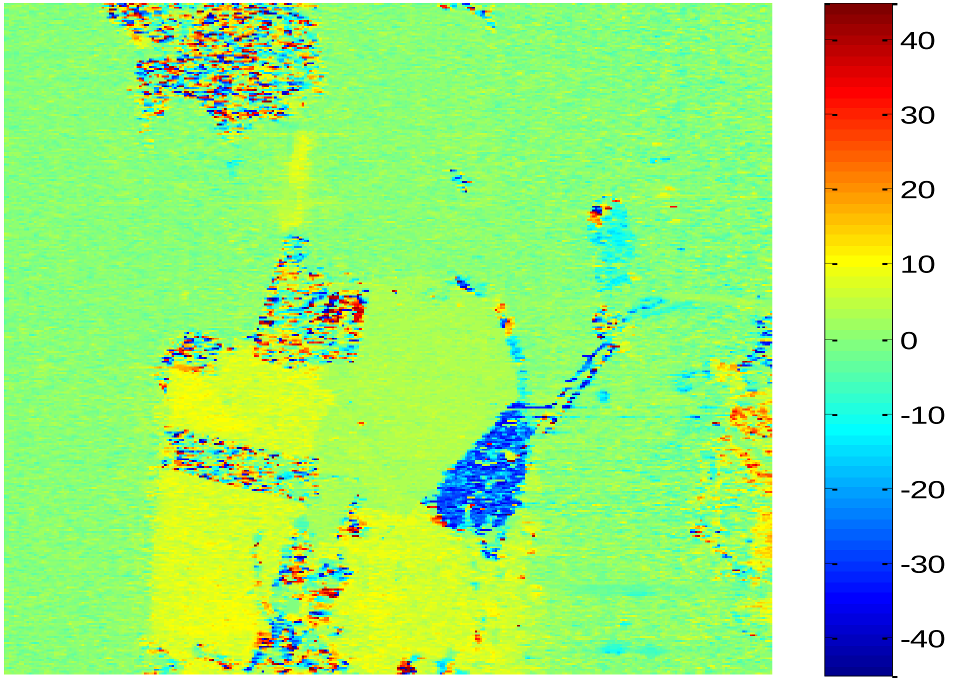

L-band ALOS-PALSAR

Noise level linked to the frequency bandwidth

X-band: very noisy over vegetation and ocean

L-band: very flat over ocean, noisy over vegetation

Use of the different polarimetric decompositions

- Coherent decompositions
  - Pauli
  - Krogager
  - Cameron
  - Touzi criterion
- Incoherent decomposition
  - Based on eigenspace: Huynen, Barnes and Holm, Cloude Pottier, Holm
  - « physical decomposition »: Freeman Durden, Yamaguchi, Van Zyl, Neumann
  - Multiplicative decomposition: Lu and Chipman

Application of polarimetry to urban areas

APPLICATIONS

Classification

3D rendering

Subsidence

Application of polarimetry to urban areas

CLASSIFICATION

Based on polarimetric parameters
Built-up detection using POLINSAR

Algorithms using POA and break of symetry

- Use of previous remarks

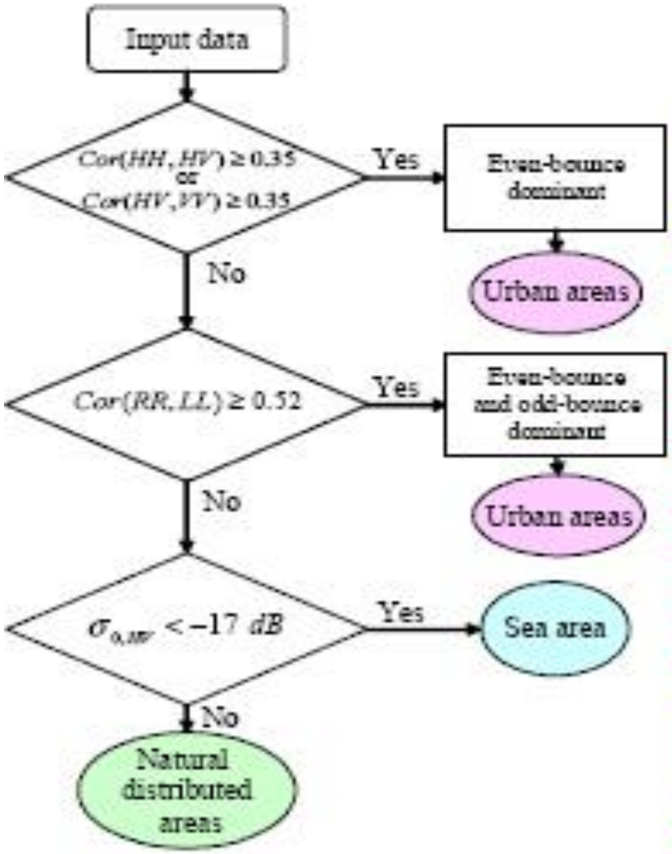

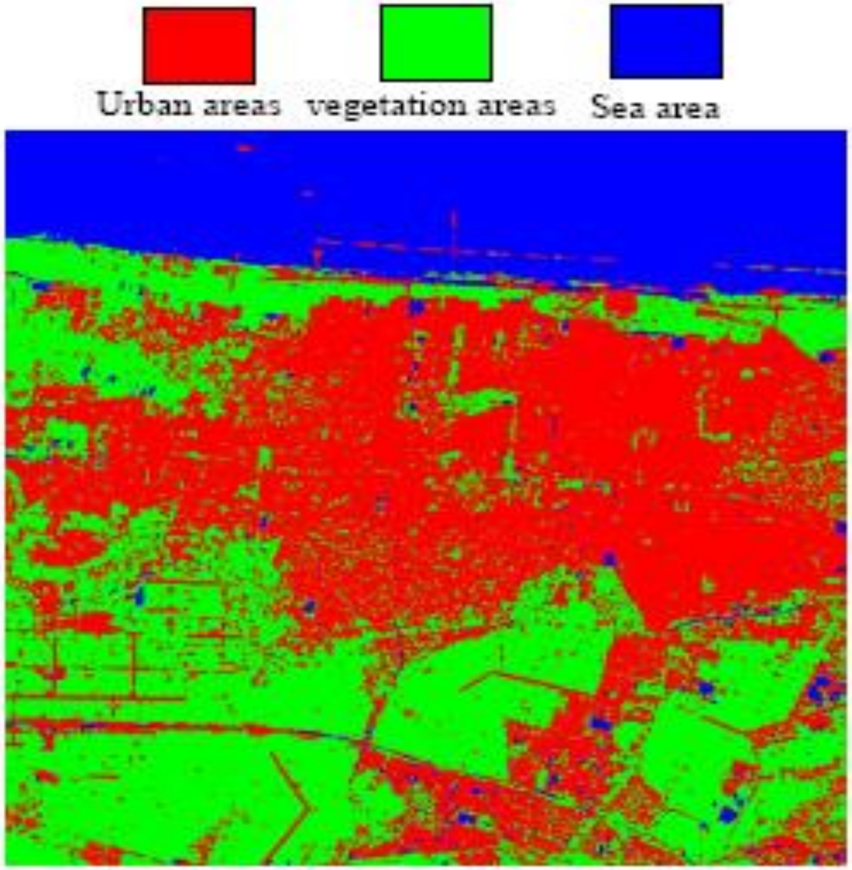

Results: classification

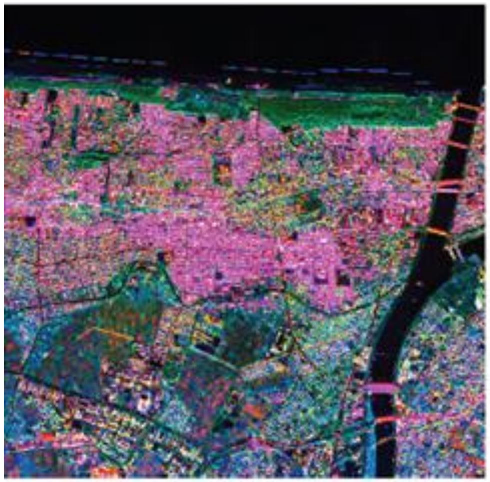

(b) 7x7

(d) Google earth image

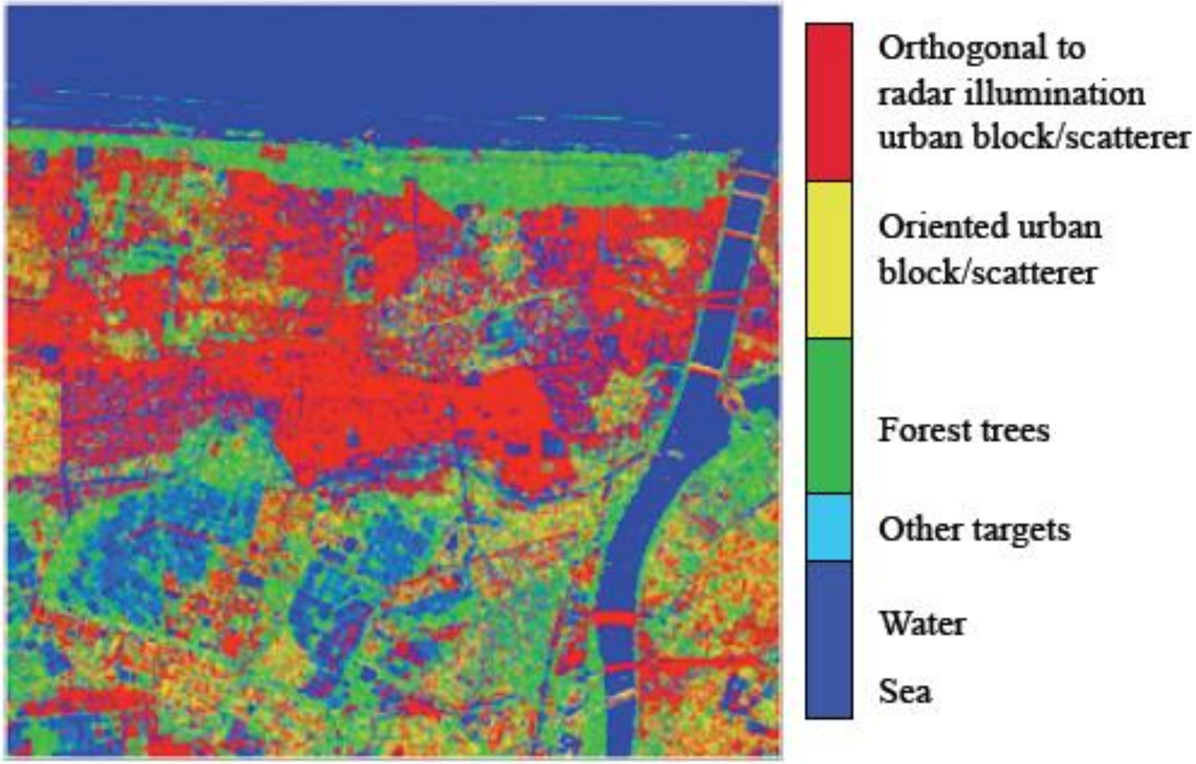

Yamaguchi versus Freeman Durden

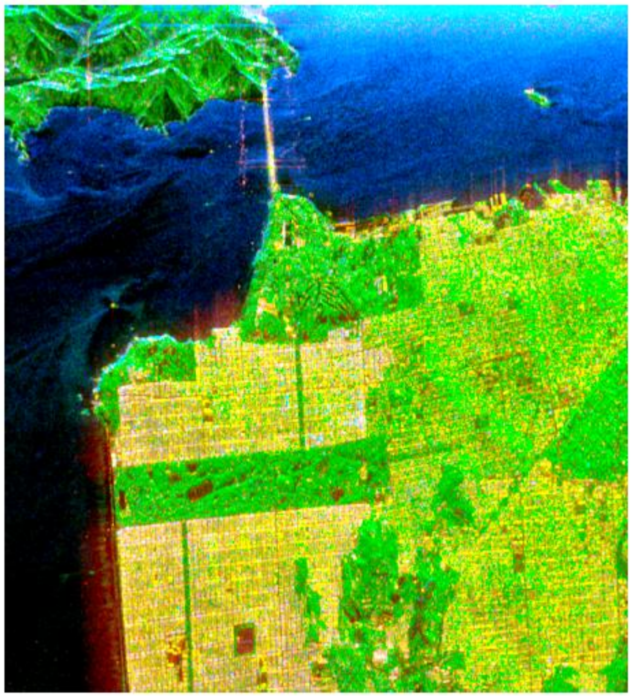

ODD *DBL* *VOL*

Freeman decomposition **Yamaguchi decomposition**

- Yamaguchi better reduces the volume component
- But still fails to identify the 45° tilted block (SOMA district)

Yamaguchi and derived decompositions

- 3-component decomposition
  - Incoherent decomposition
  - Surface, double, volume

  $T = T_{surf} + T_{double} + T_{volume}$
- 4-component decomposition
  - 3-component + helix
  - Volume scattering is modified

  $T = T_{surf} + T_{double} + T'_{volume} + T_{helix}$
- 4-component decomposition with deorientation, 4-component applied to skew-oriented buildings

Use of interferometric coherence

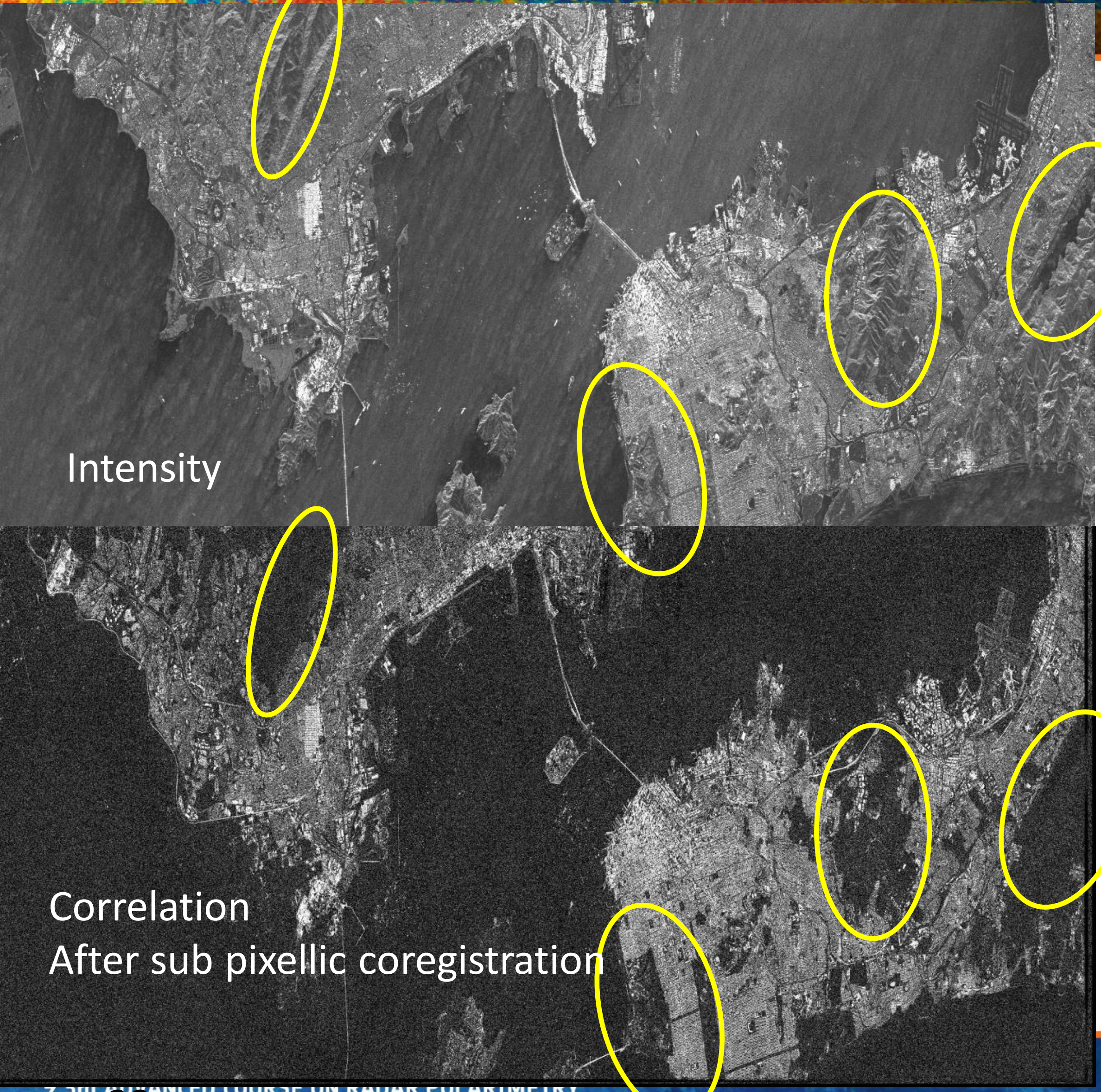

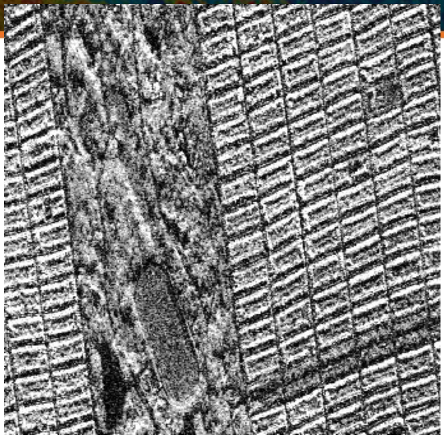

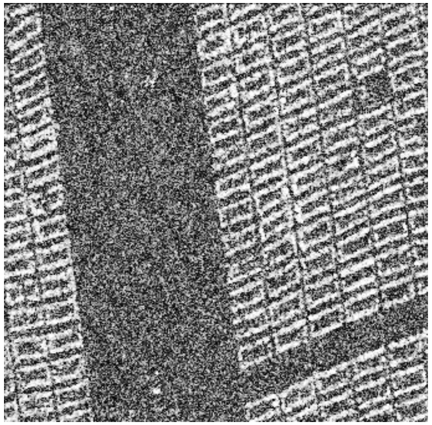

Seems to be an interesting parameters to discriminate deterministic targets!

Results: built-up detection

San Francisco

TerraSAR-X

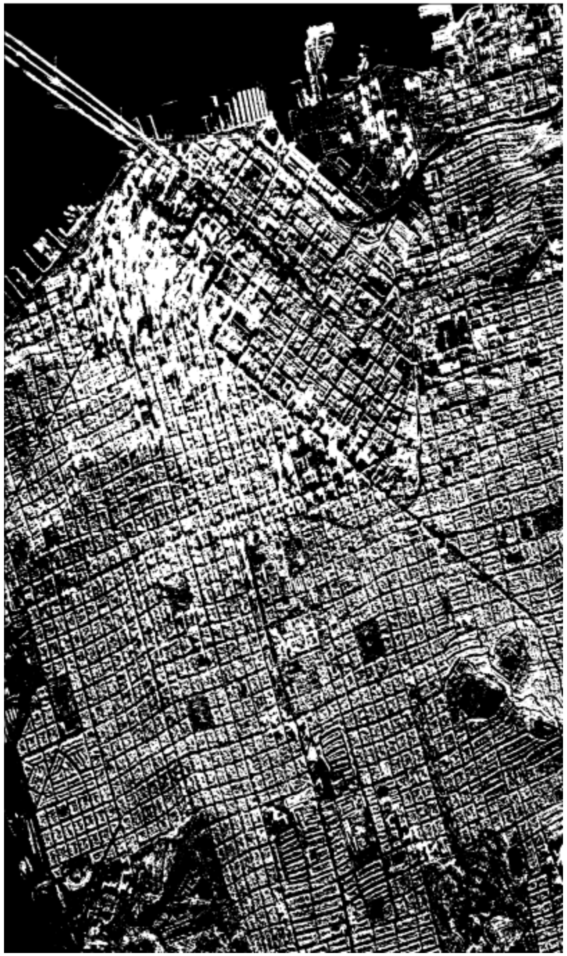

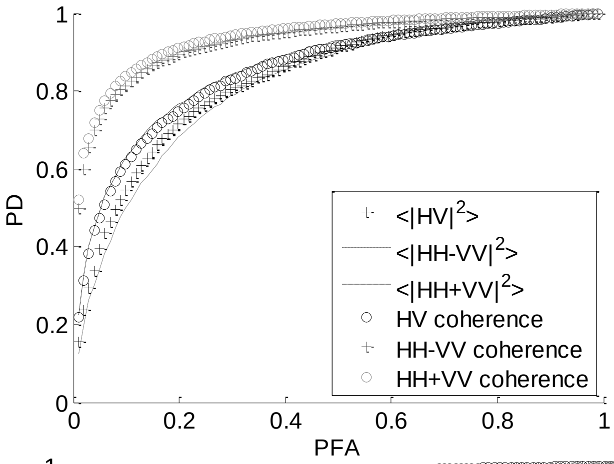

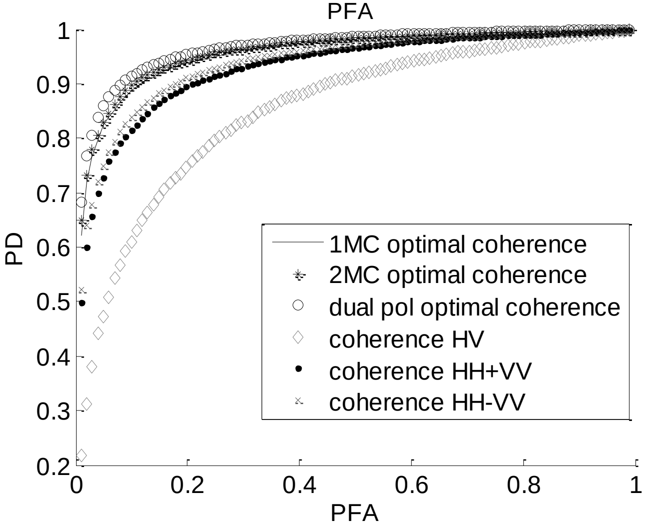

Application of polarimetry to urban areas

3D

POLINSAR
POLTOMSAR

Comparison single pass – multi pass at X-band

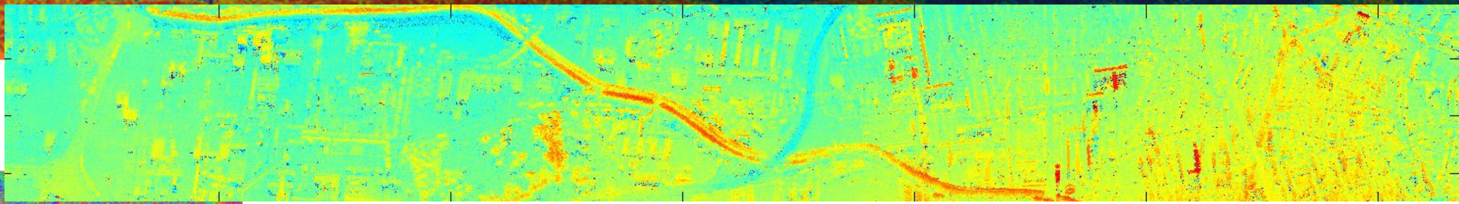

Interferometric phase at X-band over Toulouse: singla pass

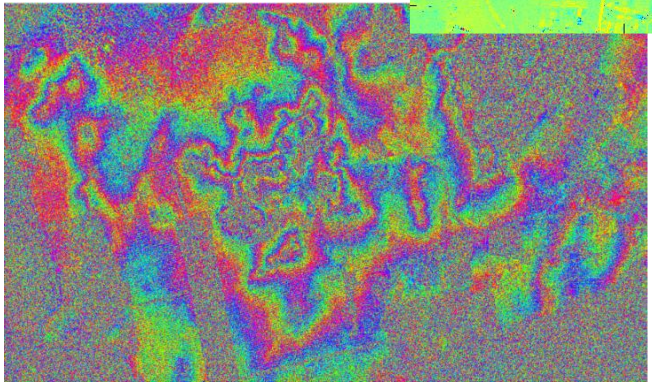

Interferometric phase at X-band over San Francisco : repeat pass

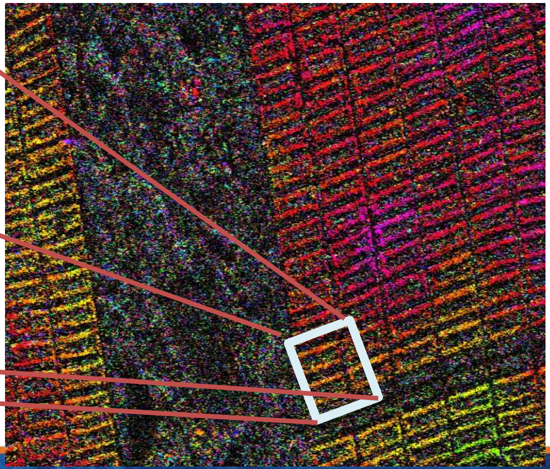

Hue : interferometric phase
Intensity : span:
Saturation : coherence level

Information avalaible only on buildings

Height estimation based on coherence shapes

Towards statistical models to predict coherence shapes

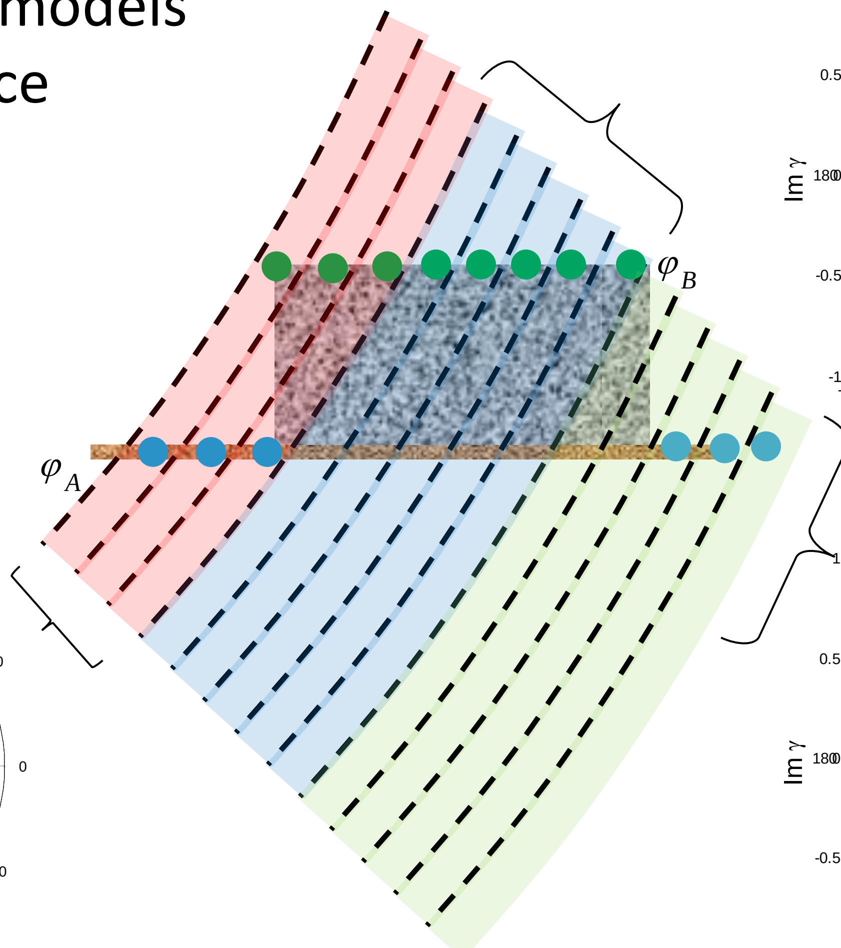

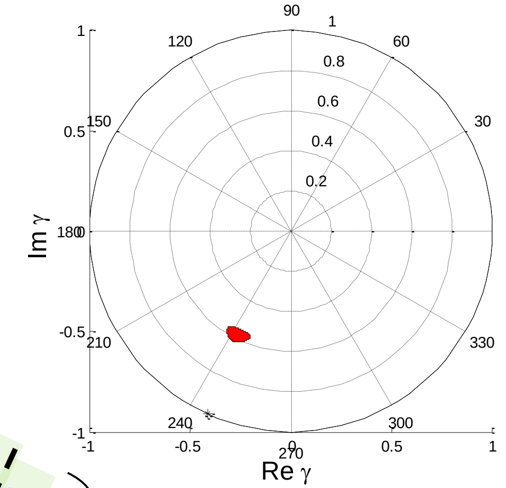

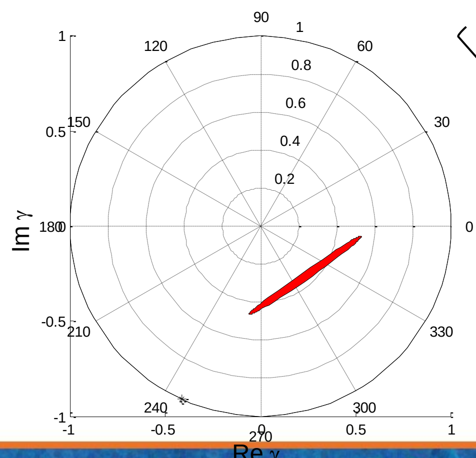

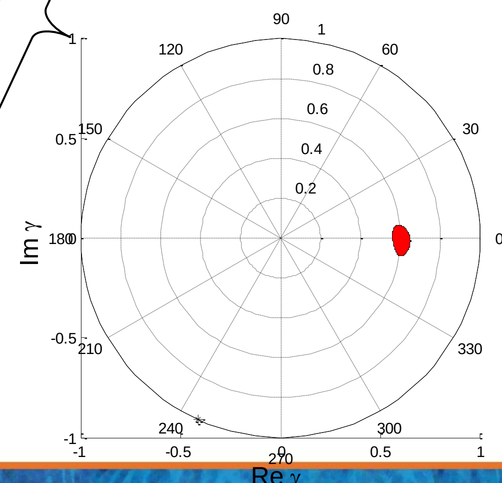

One type of scatterer

- Example : ground (1000 samples)
- Mathematical modelling

$$\mathbf{k}_{\mathbf{1}}^{\mathbf{i}} = \tau_1{}^i \mathbf{x}_1{}^i$$

$$\mathbf{k}_2^i = e^{-j\varphi_A^i} \tau_2{}^i \mathbf{x}_2{}^i$$

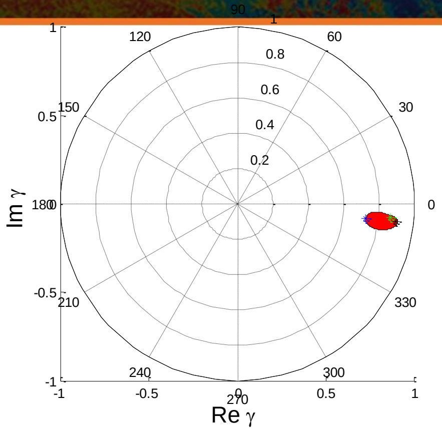

- Observation on a real case of the different contributions:

φ_A

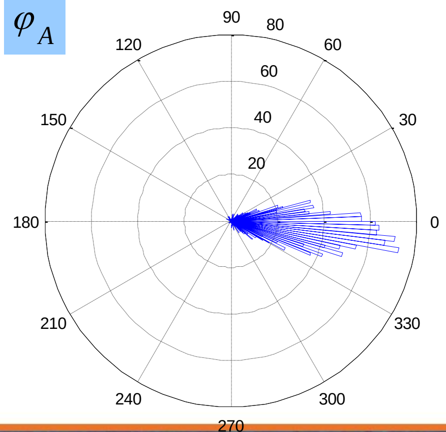

$\tau_1{}^i \approx \tau_2{}^i$

Amplitudes are perfectly correlated

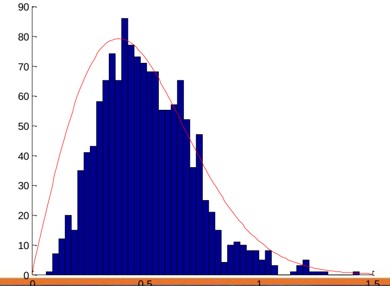

$$\mathbf{X} = \begin{pmatrix} \mathbf{x}_1 \\ \mathbf{x}_2 \end{pmatrix}$$

$$\mathbf{M} = \langle \mathbf{X}\mathbf{X}^H \rangle$$

$$\mathbf{M} \approx \begin{pmatrix} \mathbf{m} & \mathbf{m} \\ \mathbf{m} & \mathbf{m} \end{pmatrix}, \mathbf{m} \approx \begin{pmatrix} a & 0 & 0 \\ 0 & b & 0 \\ 0 & 0 & c \end{pmatrix}$$

Correlation between polarimetric pair

Statistical hypothesis

$$X = \begin{pmatrix} \mathbf{x}_1 \\ \mathbf{x}_2 \end{pmatrix}$$

- With no correlation between polarimetric vectors (1)

$$< \mathbf{x}_1{}^{i} \mathbf{x}_2{}^{jH} > = 0$$

- With two equal polarimetric vectors (maximum interferometric correlation) (2)

$$\mathbf{x}_1{}^{i} = \mathbf{x}_2{}^{i}$$

- With a covariance matrix for and non zero extradiagonal elements (3)

$$< \mathbf{x}_1{}^{i} \mathbf{x}_2{}^{jH} > \neq 0$$

Associated coherence Shape

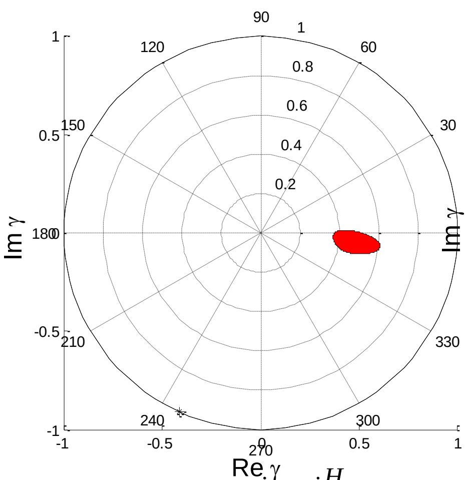

(1) $< \mathbf{x}_1{}^{i} \mathbf{x}_2{}^{jH} > = 0$

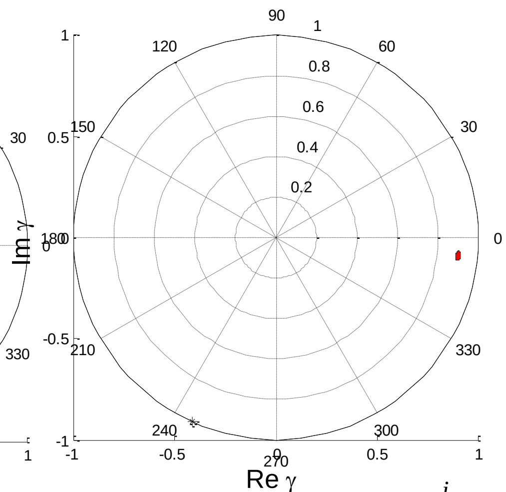

(2) $\mathbf{x}_1{}^{i} = \mathbf{x}_2{}^{i}$

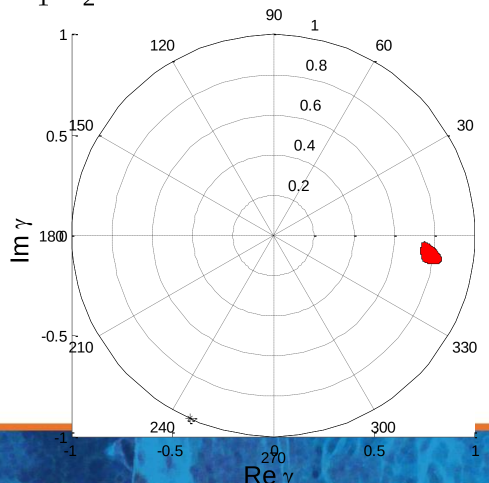

(3) $< \mathbf{x}_1{}^{i} \mathbf{x}_2{}^{jH} > \neq 0$

Modelling of a 2 bright point cell

- Mathematical modelling

$$\underbrace{\mathbf{k}_1^{\mathbf{i}} = \left[\mathbf{x}_{A1}{}^{i}, \mathbf{x}_{B1}{}^{i}\right]}_{\mathbf{S}_1} \underbrace{\begin{bmatrix} \tau_{A1}{}^{i} \\ \tau_{B1}{}^{i} \end{bmatrix}}_{\mathbf{c}_1} \qquad \mathbf{k}_2^{\mathbf{i}} = \underbrace{\left[\mathbf{x}_{A2}{}^{i}, \mathbf{x}_{B2}{}^{i}\right]}_{\mathbf{S}_2} \underbrace{\begin{bmatrix} e^{-j\varphi_A^i} & 0 \\ 0 & e^{-j\varphi_B^i} \end{bmatrix}}_{\mathbf{D}} \underbrace{\begin{bmatrix} \tau_{A2}{}^{i} \\ \tau_{B2}{}^{i} \end{bmatrix}}_{\mathbf{c}_2}$$

- Mixture of two different polarimetric statistics on points A and B:

$$\mathbf{S}_1 = \left[\mathbf{x}_{A1}{}^{i}, \mathbf{x}_{B1}{}^{i}\right]$$

$$\mathbf{S}_2 = \left[\mathbf{x}_{A2}{}^{i}, \mathbf{x}_{B2}{}^{i}\right]$$

Point A

$$\mathbf{X}_A = \begin{pmatrix} \mathbf{x}_{1A} \\ \mathbf{x}_{2A} \end{pmatrix} \qquad \mathbf{M}_A = \langle \mathbf{X}_A \mathbf{X}_A{}^{H} \rangle$$

Point B

$$\mathbf{X}_B = \begin{pmatrix} \mathbf{x}_{1B} \\ \mathbf{x}_{2B} \end{pmatrix} \qquad \mathbf{M}_B = \langle \mathbf{X}_B \mathbf{X}_B{}^{H} \rangle$$

Estimation of coherence on real data

- Ground segments and building segments

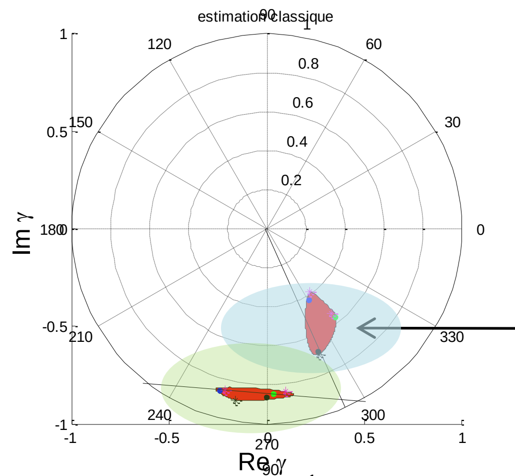

Bare soil segments

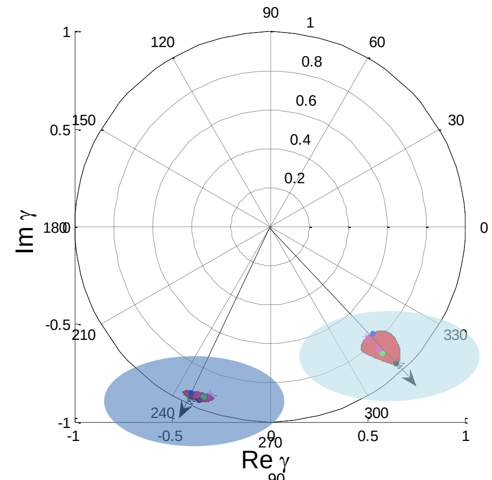

Building segments without internal polarimetric diversity

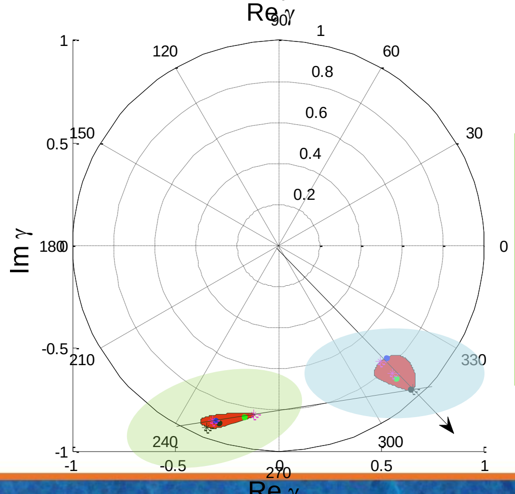

Building segments with polarimetric diversity

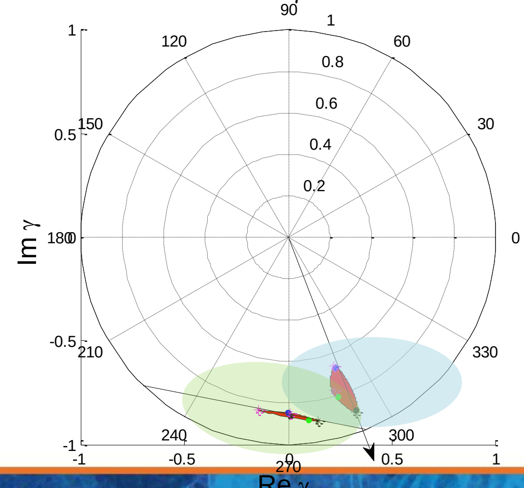

Height estimation

Ground truth	estimated height
22	23.7
19	16.3
16	13.9
23	18.4
24	24.8
24	24.2
24	25.3
10	13.9
23	24.6
21	19.5

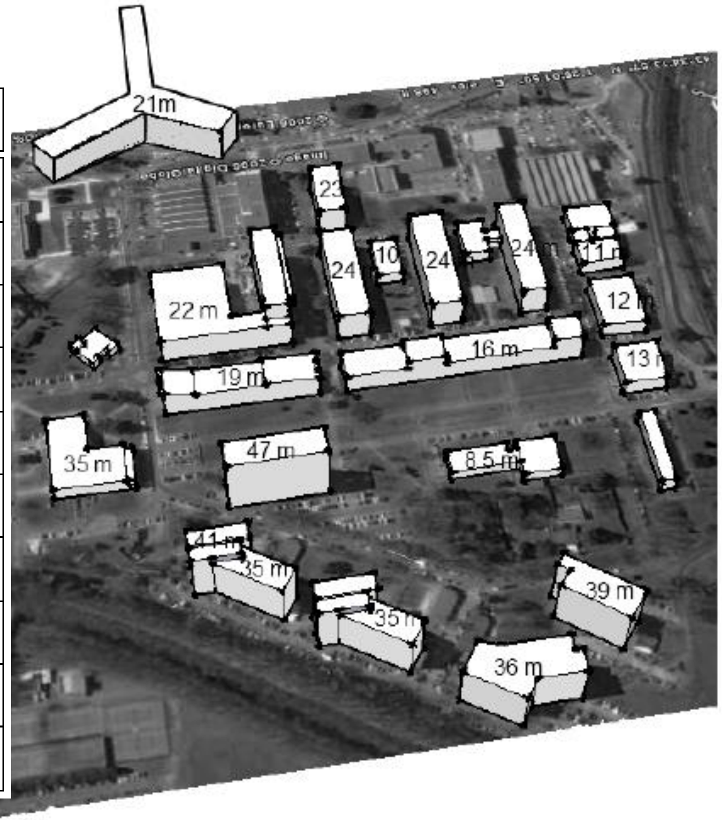

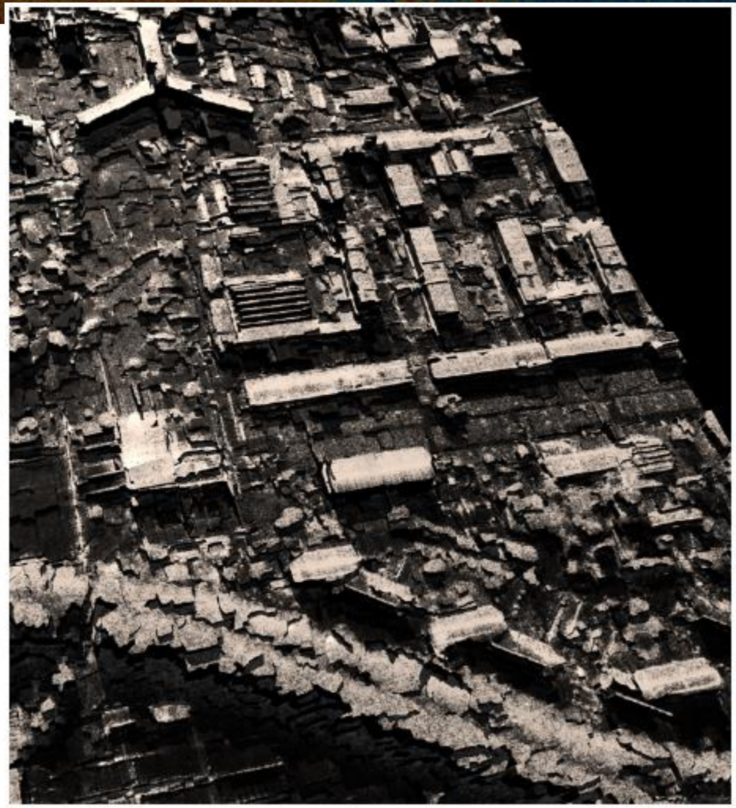

- données Google 3D INSA/Université
- Segmentation et estimation 3D

Root mean squared error

Results: 3D rendering

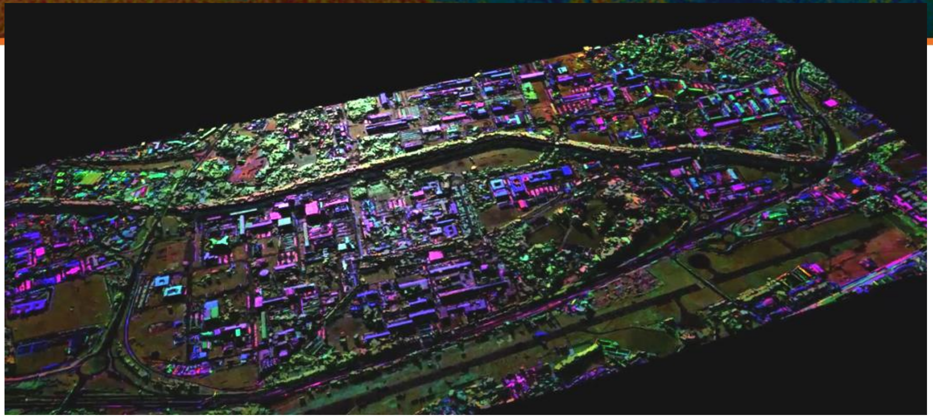

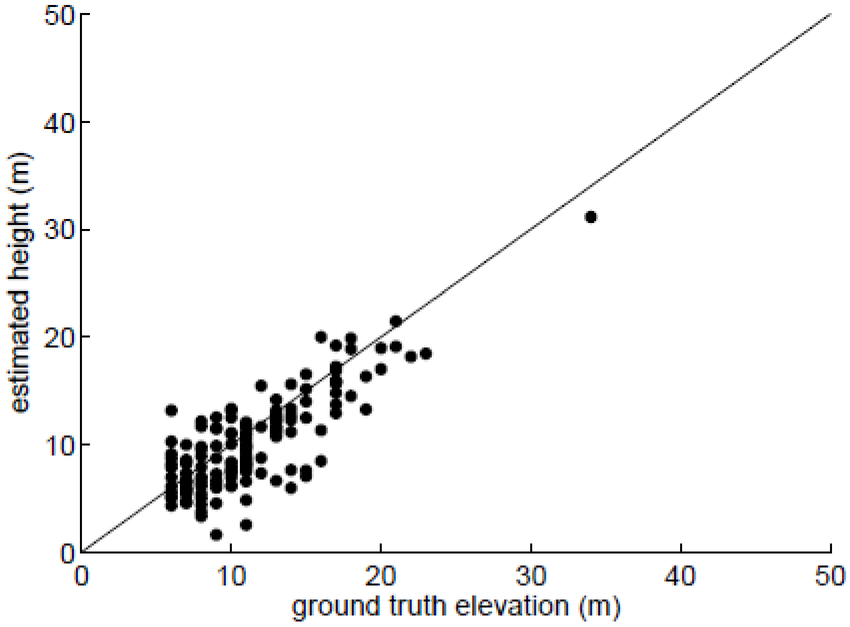

Polarization use	Ground truth height – estimated height (m)	RMSE (m)
HH+VV	2,57	3,89
HH-VV	2,76	4,60
HV	2,23	3,79
Dual pol	1,20	3,76
Full pol	1,20	2,87

Tomography

- MB Insar Approach : heights, layover sources
- Polarimetry + InSAR :

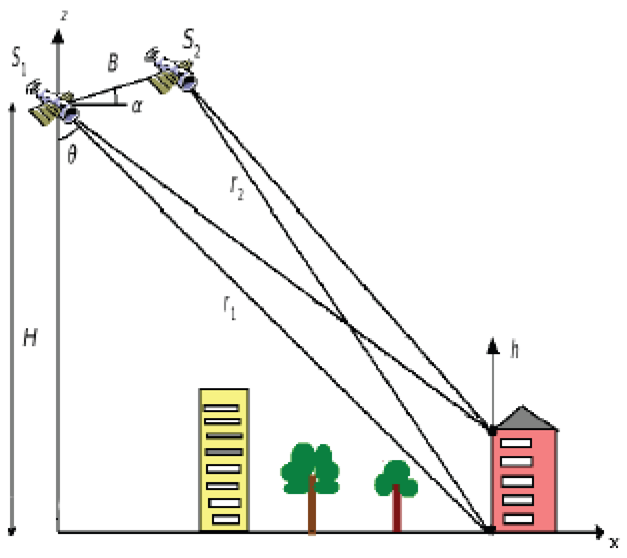

Example of tomograms

- E-SAR L-band

Pauli color-coded urban scene

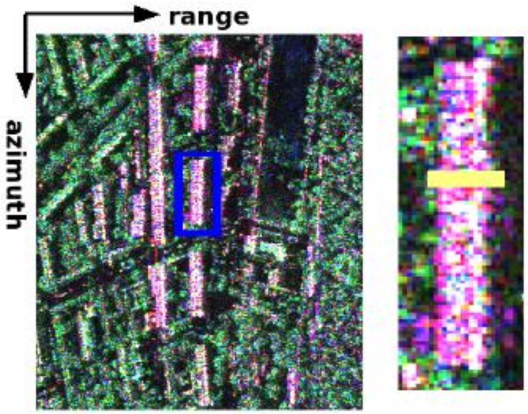

MUSIC pseudo-tomogram (order=1)

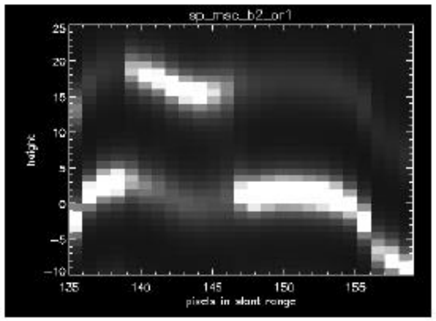

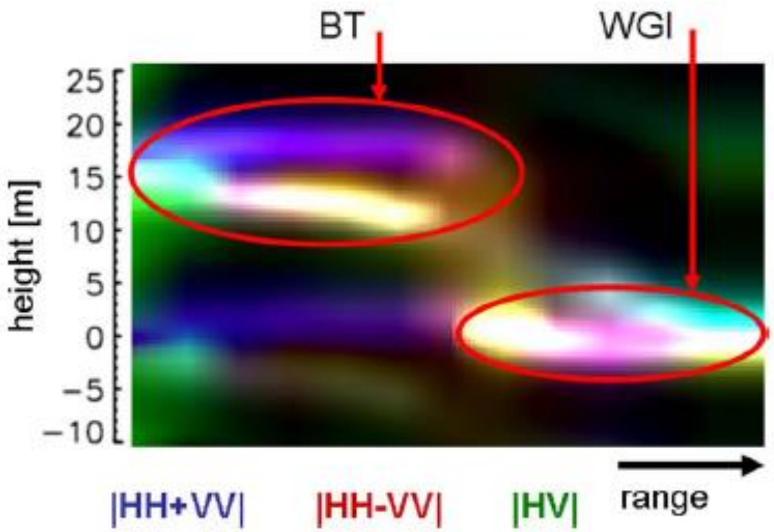

MUSIC discrete pseudo-tomogram (order=1)

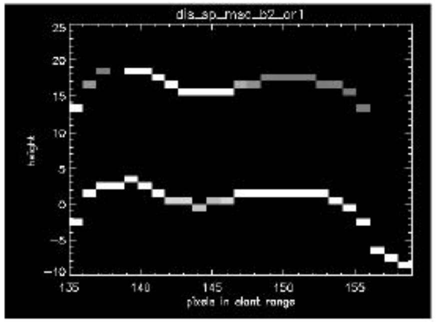

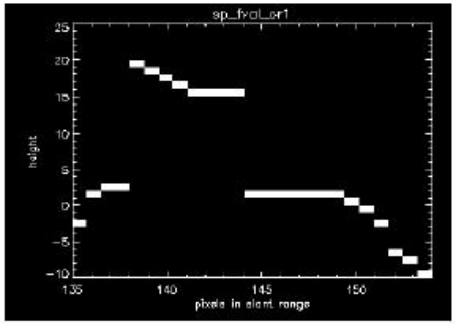

Pseudotomographic slices of the optimal MUSIC scattering mechanisms

Refined characterization of building height and scattering mechanisms

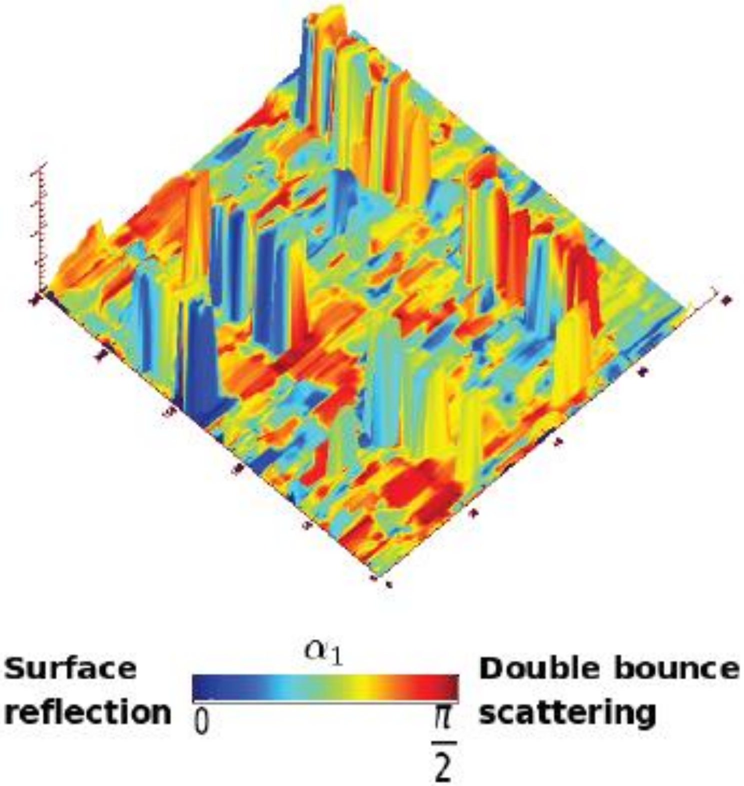

Results: tomography

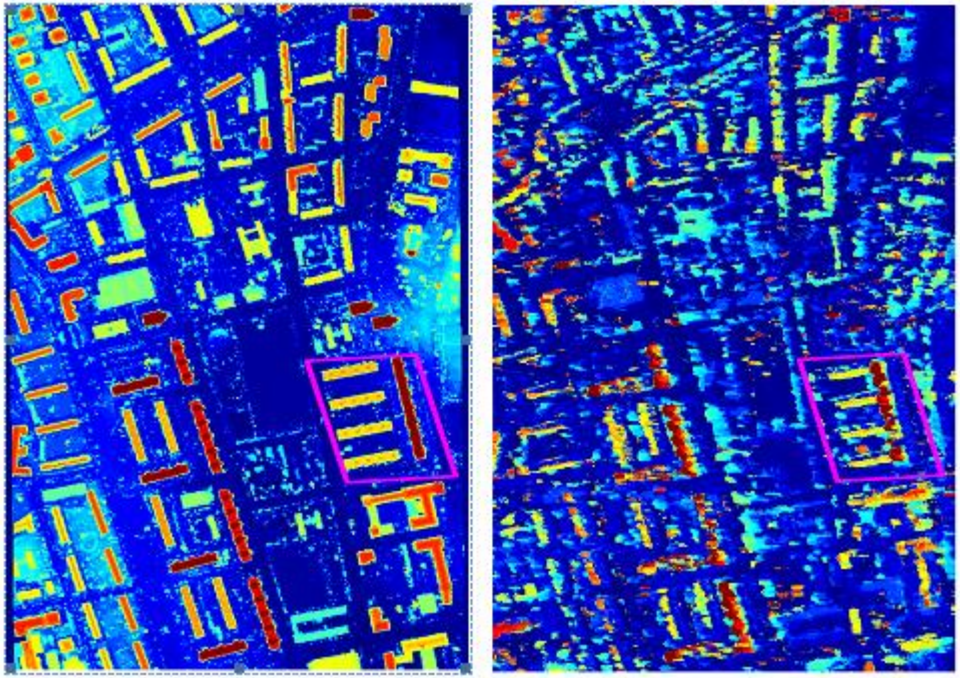

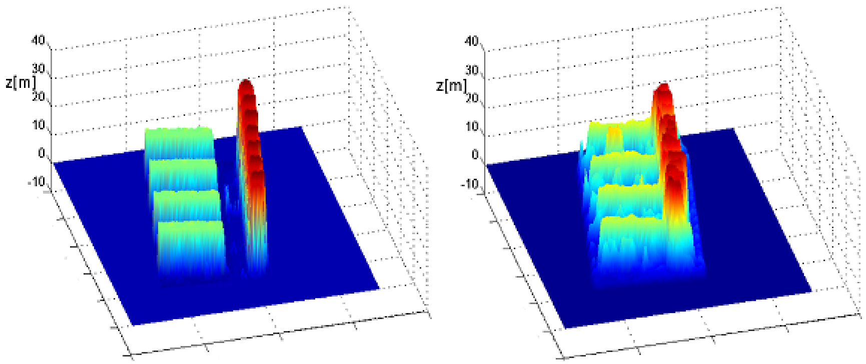

3-D reconstruction: LiDAR (left) and FP-NSF estimator (right).

Application of polarimetry to urban areas

SUBSIDENCE

subsidence

- Why subsidence in urban areas ? may be caused by factors including
  - groundwater extraction
  - load of constructions
  - natural consolidation of alluvium soil
  - geotectonic subsidence

Bologne

Astrium GEO-Information Services

Monitoring of land subsidence

is required for

- groundwater extraction regulation,
- effective flood control and seawater intrusion,
- conservation of environment
- construction of infrastructure, and spatial development planning in general.

Contribution of POLSAR to PSI

- Persistent Scatteter Interferometry yields ground deformation values, along time, for a set of pixels selected (PSC: persistent scatterer candidates) from the images
- Key point: A good density and spatial distribution of the PSC is required for:
  - InSAR processing (e.g. phase unwrapping)
  - Model adjustment (arcs and integration)
  - Atmospheric phase screen (APS) consistent estimation/removal
- Selection of PSC: pixels whose phase is stable (not noisy) in time
  - Problem: we cannot trust directly in the measured phases
  - Selection criteria:
    - Low amplitude dispersion (SLC images)
    - High average interferometric coherence (multi-looked interferograms)

Contribution of POLSAR to PSI

1st contribution of polarimetry to PSI:
increase the number of PSC by optimising the quality criteria

Example in Murcia (Spain), with 45 TerraSAR-X images HHVV

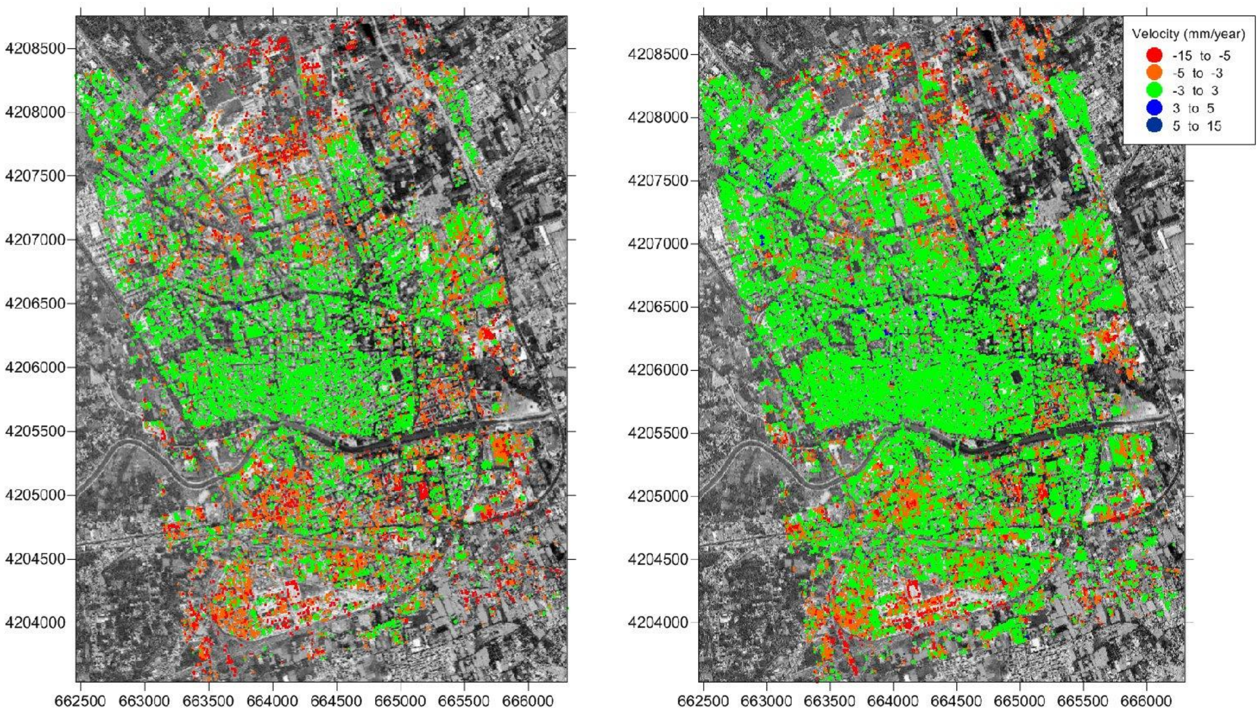

VV OPT

Increase in number of pixels over single-pol:

- Coherence: 60%
- Amplitude: 170%

	HH	VV	HH+VV	HH−VV	Optimum
Whole scene	28.29%	24.07%	21.79%	31.00%	38.57%
Urban area	41.47%	34.02%	32.20%	45.23%	55.82%
Rural area	15.15%	10.04%	8.99%	14.25%	18.20%

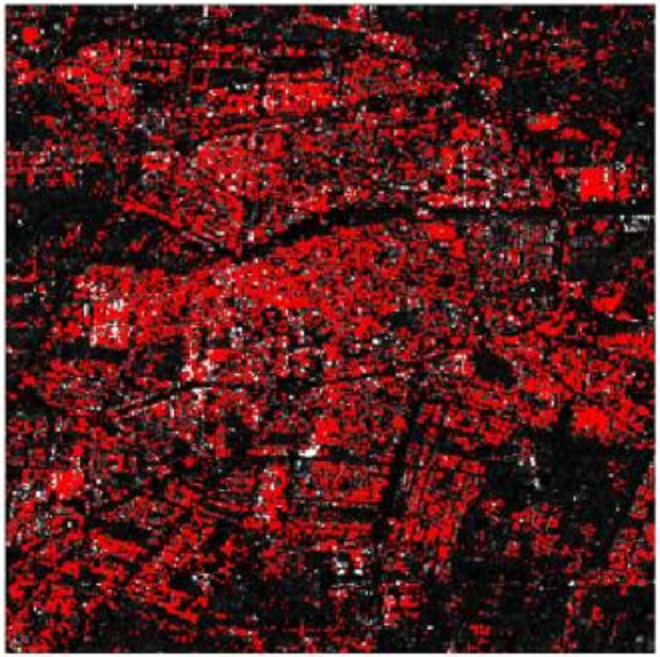

VV
Pixels selected = 24.07%

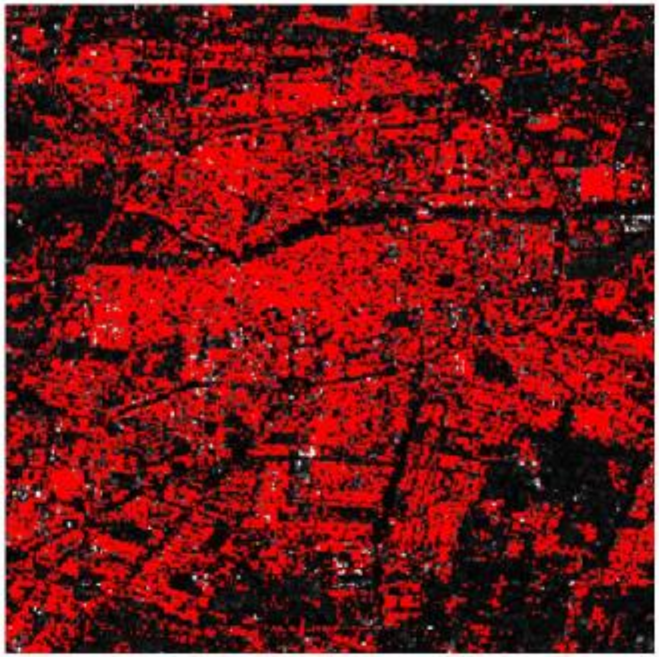

OPT
Pixels selected = 38.57%

Results: ground deformation

Number of Reliable Pixels Selected (Coherence Stability)a	
Method	**Number of pixels**
hh	**6431 (3.3%)**
hv	**5026 (2.6%)**
vv	**5014 (2.6%)**
Best	**11931 (6.1%)**
SOM	**13894 (7.1%)**
ESM	**17281 (8.9%)**

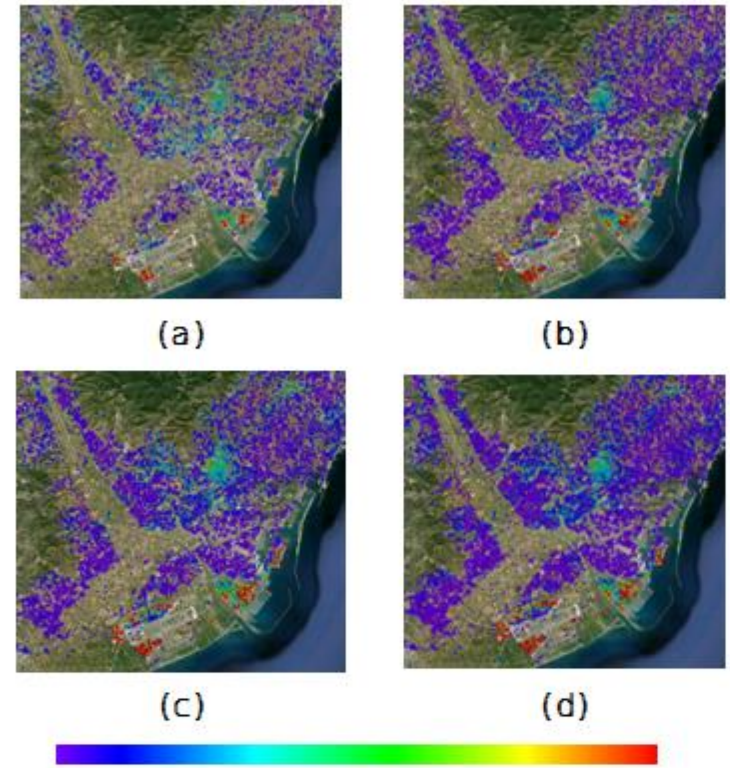

0 cm/year 0.5 cm/year

(a) HH
(b) Best
(c) SOM
(d) ESM optimization methods.

Application of polarimetry to urban areas

CONCLUSIONS

Conclusions

Classification

- X-band: very recent development. In this context, polarimetry only seems to become less effective for discriminating built-up areas. Essential contribution of polarimetry in the detection of built-up areas is the optimization of the PolInSAR coherence. It is used to discriminate targets based on their speed of temporal decorrelation.

- As regards the contribution of HV versus dual mode pol HH / VV, the situation is less clear, essentially due to the poor SNR in the HV channel of TerraSAR-X data.

- Still at X-band, the correlation coefficient in the circular polarization basis contains useful information on objects. It can be used for classification, derivation of surface slope, polarization orientation angle, among others. Not applicable to single/dual polarimetric data sets.

Conclusions

3D rendering (POLINSAR – Tomography)

- Polarimetry improves the precision obtained on the height estimates of a factor of two. The mean squared error has been reduced also.
- Full polarimetry improves the RMSE versus dual polarimetry
- Among all single polarizations, the HV gives the best results
- Errors and estimation difficulties are mainly:
  - Bad choice of the population of pixels belonging to the roof.
  - Sources of polarimetric decorrelation of interferometric noise.

Conclusions

Subsidence

- The polarimetric optimization methods demonstrate its capability to enhance the quality of DInSAR and PSI results:

  - higher density of pixels compared with the single polarization case.
  - quality of the interferometric phase is also improved, leading to more precise deformation maps

- First experiments with full-pol data show a more significant improvement than dual-pol, increasing the density of selected pixels up to twice with respect to dual-pol optimised data, and more than four times with respect to single-pol.

- Including the HV channel in the processing adds a great deal of information, given the important cross-polar response coming from tilted dihedrals in urban areas (oriented buildings).